Observations of mixing and transport on a steep beach

Brown, Jenna A.; MacMahan, Jamie H.; Reniers, Ad J.H.M.; Thornton, Ed B.; Shanks, Alan L.; Morgan, Steven G.; Gallagher, Edie L.

DOI
10.1016/j.csr.2019.03.009

Publication date
2019

Document Version
Final published version

Published in
Continental Shelf Research

Citation (APA)
Brown, J. A., MacMahan, J. H., Reniers, A. J. H. M., Thornton, E. B., Shanks, A. L., Morgan, S. G., & Gallagher, E. L. (2019). Observations of mixing and transport on a steep beach. *Continental Shelf Research*, *178*, 1-14. https://doi.org/10.1016/j.csr.2019.03.009

Continental Shelf Research 178 (2019) 1–14

Contents lists available at ScienceDirect

Continental Shelf Research

journal homepage: www.elsevier.com/locate/csr

Observations of mixing and transport on a steep beach

Jenna A. Brown[a,*], Jamie H. MacMahan[a], Ad J.H.M. Reniers[b,c], Ed B. Thornton[a], Alan L. Shanks[d], Steven G. Morgan[e], Edie L. Gallagher[f]

[a] Department of Oceanography, Naval Postgraduate School, Monterey, CA, 93943, USA
[b] Rosenstiel School of Marine and Atmospheric Science, University of Miami, 4600 Rickenbacker Causeway, Miami, FL, 33149, USA
[c] Department of Hydraulic Engineering, Delft University of Technology, Stevinweg 1, 2628, CN, Delft, the Netherlands
[d] Oregon Institute of Marine Biology, University of Oregon, Charleston, OR, 97420, USA
[e] Bodega Marine Laboratory, University of California, Davis, Bodega Bay, CA, 94923, USA
[f] Department of Biology, Franklin and Marshall College, Lancaster, PA, 17604, USA

ARTICLE INFO

Keywords:
Steep beach
Surfzone
Dye
Mass transport
Dispersion
Diffusion

ABSTRACT

Surfzone mixing and transport on a sandy, steep (~1/8 slope), reflective beach at Carmel River State Beach, California, are described for a range of wave and alongshore flow conditions. Depth-limited wave breaking occurred close to the shore due to the steepness of the beach, creating a narrow surf/swash zone (~10 m wide). Fluorescent Rhodamine dye was released as a slug in the surfzone, and the temporal and spatial evolution was measured using in-situ dye sensors. Dye concentration measured as a function of time reveals sharp fronts that quickly decay resulting in narrow peaks near the dye release, which subsequently broaden and decrease in peak concentration with alongshore distance. The measurements indicate two stages of mixing and transport occur inside the surfzone on the steep beach. 1) In the near-field (< 50 m downstream of the dye release location), the dye fully mixed throughout the water column after a few incident waves then continued to disperse in two dimensions, with both advection and diffusion processes being important. 2) In the far-field (> 50 m downstream from the dye release location), the mass transport was dominated by advection. The distance to the far-field is much shorter in the alongshore on a steep beach compared with a dissipative beach. Estimates of cross-shore and alongshore diffusion coefficients (κ_x, κ_y) were found to be similar in magnitude within the surfzone. Outside the surfzone in the far-field, the results suggest that the mixing processes are independent of those inside the surfzone. The mixing and transport of material observed on this steep beach are found to be analogous to that previously measured on dissipative beaches, however the diffusion coefficients within and outside the surfzone were found to be smaller on this steep beach.

1. Introduction

The mixing and transport of material in the nearshore, including suspended sediment, pollutants, biological matter, and nutrients, influences beach composition, water quality, and ecosystem stability. There have been few field studies on mass transport and cross-shore exchange across the surfzone boundary, and most have occurred on wide, dissipative beaches in southern California (Inman et al., 1971; Boehm, 2003; Grant et al., 2005; Clark et al., 2010; Hally-Rosendahl et al., 2014, 2015) and on a rip-channeled beach in Monterey, California (MacMahan et al., 2010; Brown et al., 2015). A number of numerical experiments have evaluated material exchange and the offshore extent on dissipative beaches associated with stationary rip currents (Reniers et al., 2009; Reniers et al., 2010; Castelle and Coco, 2013; Fujimura et al., 2013; Castelle et al., 2014; Fujimura et al., 2014) and transient rip currents (Suanda and Feddersen, 2015; Hally-Rosendahl and Feddersen, 2016; Kumar and Feddersen, 2017a, 2017b, 2017c). Dissipative beaches support communities with large human populations, where an understanding of the mixing and transport of pollutants has both health and economic relevance (Grant et al., 2005; Given et al., 2006; amongst others). In contrast, steep reflective beaches usually do not support recreational activities owing to their hazardous shore break; however, dense and diverse communities of organisms are often found in these environments (Morgan et al., 2018). Therefore, steep beach experiments can lead to increased knowledge of exchange processes that are important to these communities, such as biological

* Corresponding author. U.S. Geological Survey St. Petersburg Coastal and Marine Science Center, 600 4th St. S, St. Petersburg, FL, USA.
E-mail addresses: jennabrown@usgs.gov (J.A. Brown), jhmacmah@nps.edu (J.H. MacMahan), a.j.h.m.reniers@tudelft.nl (A.J.H.M. Reniers), thornton@nps.edu (E.B. Thornton), ashanks@uoregon.edu (A.L. Shanks), sgmorgan@ucdavis.edu (S.G. Morgan), edith.gallagher@fandm.edu (E.L. Gallagher).

https://doi.org/10.1016/j.csr.2019.03.009
Received 28 December 2017; Received in revised form 15 March 2019; Accepted 18 March 2019
Available online 23 March 2019
0278-4343/ Published by Elsevier Ltd.

recruitment. In general, a better understanding of how material is dispersed on beaches with varying morphology and wave and current conditions is needed.

Mixing and transport in the surfzone results from several physical processes with distinctive temporal and spatial scales, which can be separated into two dominant mechanisms: 1) diffusion, which describes the spreading of material due to turbulent motions, and 2) advection, which describes the bodily transport of material due to wave-driven surfzone currents. Fluorescent dye tracers have been used in field studies to examine surfzone mixing and transport on wide, dissipative beaches, focusing on alongshore dispersion (Harris et al., 1963; Inman et al., 1971; Boehm, 2003; Grant et al., 2005), cross-shore dispersion (Clark et al., 2010), or cross-shore exchange between the surfzone and inner shelf (Hally-Rosendahl et al., 2014, 2015). Surfzone dye was observed to be vertically well mixed (Hally-Rosendahl et al., 2014, 2015), and experienced initial 2-D horizontal dispersion (cross-shore and alongshore) and transport until the surfzone was saturated (approximately uniform cross-shore concentration). Once the surfzone was saturated (at a distance 100 m to over 1 km alongshore from the dye release location), the dye was transported by advection in the alongshore direction (Harris et al., 1963; Inman et al., 1971; Grant et al., 2005; Clark et al., 2010). In some cases, dye was visually observed (Grant et al., 2005) and measured in-situ and remotely-sensed (Hally-Rosendahl et al., 2014, 2015) to be transported to the inner shelf by transient rip currents, which has also been numerically modeled (Suanda and Feddersen, 2015; Hally-Rosendahl and Feddersen, 2016; Kumar and Feddersen, 2017a, 2017b, 2017c).

The amounts of alongshore transport and cross-shore exchange occurring on these dissipative beaches were estimated using simple models of mass transport and tracer observations. A conceptual transport model suggests alongshore advection dominates both alongshore mixing and cross-shore mixing (Boehm, 2003; Grant et al., 2005), and field measurements of alongshore mass transport on dissipative beaches indicate a decay of tracer as a function of distance along the shoreline from the release point, either exponentially (Inman et al., 1971; Grant et al., 2005) or following a power-law (Hally-Rosendahl et al., 2014, 2015). On separate alongshore uniform, dissipative beaches with predominant alongshore currents, Hally-Rosendahl et al., (2014) found the cross-shore transport of dye from the surfzone to the inner shelf was approximately 40% of the alongshore surfzone transport over a distances greater than 0.5 km from the tracer source, consistent with observations by Grant et al., (2005). Using a two-box model of tracer transport between the surfzone and the inner shelf, cross-shore exchange velocity was estimated to be 0.009–0.012 m/s and was attributed to transient rip currents (Hally-Rosendahl et al., 2014, 2015). Evidence of dye within the surfzone at long times after the dye release indicate dye was recycled back into the surfzone from the inner shelf (Hally-Rosendahl et al., 2014), suggesting that inner shelf tracer accumulation and recycling back into the surfzone are important considerations when examining the downstream evolution of surfzone-sourced tracers, and that the surfzone boundary should not be considered no-flux when computing the mass transport.

Surfzone mixing on a dissipative beach was examined by Clark et al., (2010) using tracer measurements and a Fickian diffusion model. Cross-shore surfzone diffusion coefficient, κ_x, was estimated using a numerical solution to the 2-D advection-diffusion equation, with a shoreline dye point source, alongshore-uniform planar beach, and assuming a no-flux boundary at the shoreline. The model was applied to ensemble-averaged cross-shore profiles of tracer concentration inside the surf zone resulting in estimates of $\kappa_x = 0.5–2.5\,m^2\,s^{-1}$, which was attributed to surfzone eddies forced by shear instabilities or finite-crest-length wave breaking. Gradients in dye concentration observed at the seaward edge of the surfzone (Clark et al., 2010) and alongshore-patchiness of dye on the inner shelf that was locally advected from the surfzone (Hally-Rosendahl et al., 2014), are consistent with weak horizontal mixing and lower diffusivity outside the surfzone (Harris et al., 1963; Inman et al., 1971).

Surfzone diffusivities on dissipative beaches have also been estimated using surface drifters, with asymptotic (long time) $\kappa_x = 0.7–1.5\,m^2\,s^{-1}$ and $\kappa_y = 2.0–4.5\,m^2\,s^{-1}$ found for an alongshore uniform beach (Spydell et al., 2007), and asymptotic $\kappa_x = 0.9–2.2\,m^2\,s^{-1}$ and $\kappa_y = 2.8–3.9\,m^2\,s^{-1}$ found for a rip-channeled beach (Brown et al., 2009). Drifter observations outside the surfzone indicate similar diffusivities for an alongshore uniform beach (Spydell et al., 2007) and slightly smaller diffusivities (asymptotic $\kappa_x = 0.3–1.7\,m^2\,s^{-1}$ and asymptotic $\kappa_y = 0.4–5.0\,m^2\,s^{-1}$) for a rip-channeled beach (Brown et al., 2015), compared to inside the surfzone. On all beaches, asymptotic diffusivity values were reached faster within the surfzone. At long times outside the surfzone, drifters spread more quickly in the alongshore than the cross-shore, with $\kappa_y > \kappa_x$, for alongshore uniform beaches (Spydell et al., 2007) and during combined alongshore and cross-shore exchange for a rip-channeled beach (Brown et al., 2015). However, cross-shore diffusivity was similar to (Brown et al., 2009) or slightly greater than (Brown et al., 2015) alongshore diffusivity during rip current cross-shore exchange conditions for a rip-channeled beach. The surface drifter estimates of surfzone diffusion coefficients are consistent with the dye concentration results for dissipative beaches.

In this work, field observations of the 2-D mixing and transport processes that occur on a sandy, steep, reflective beach are investigated and compared with the findings on dissipative beaches. Dye is used here as drifters do not perform well in the energetic, narrow surfzone of a steep beach. In-situ vertical profile current measurements are used to relate the measured surfzone velocities to those of a typical swash zone, and to examine the presence of an undertow cross-shore velocity profile inside and outside the surfzone (Section 3). Dye was released as a point source in the narrow surfzone and the temporal and spatial evolution was measured (Section 4). Alongshore mixing and transport inside the surfzone are examined in Section 4.3, and cross-shore mixing inside and outside the surfzone are examined in Section 4.4. Mixing and transport on the steep beach was found to occur in two stages and is discussed in Section 5.1, and the effects of the local bathymetry on transport and cross-shore exchange at this particular field site are discussed in Section 5.2. A summary of the mixing and transport on this steep beach is given in Section 6.

2. Field experiment

2.1. Field site

Field observations were obtained during June and July 2011 on a sandy, steep, reflective beach at Carmel River State Beach (CRSB), California. Bathymetry was surveyed multiple times throughout the experiment using a kinematic Global Positioning System (GPS) mounted to an electric kayak equipped with an echosounder to measure the offshore and to a backpack carried by a walking person to measure the dry beach. The beach step was measured by a person swimming cross-shore transects with a survey rod affixed with a GPS atop at numerous alongshore locations. The survey data were combined and interpolated to a unified bathymetric grid. A local coordinate system is used where the origin is in the center of the beach, and the cross-shore coordinate, x, is positive offshore and the alongshore coordinate, y, is positive to the south (Fig. 1).

The alongshore-averaged, cross-shore beach profile was composed of a 1/8 subaerial beach slope, a steep 1/3 subaqueous beach step, and a 1/19 subaqueous offshore profile (Fig. 1). Due to the steepness of the beach, depth-limited wave breaking occurred very close to the shore, resulting in a narrow surfzone that was intermittent in width at the frequency of the sea-swell waves. The plunging-collapsing/surging breakers were effectively the run-up associated with the swash zone that alternately wets and dries the beach. Therefore, the surfzone on this steep beach is more of a large swash zone rather than a typical

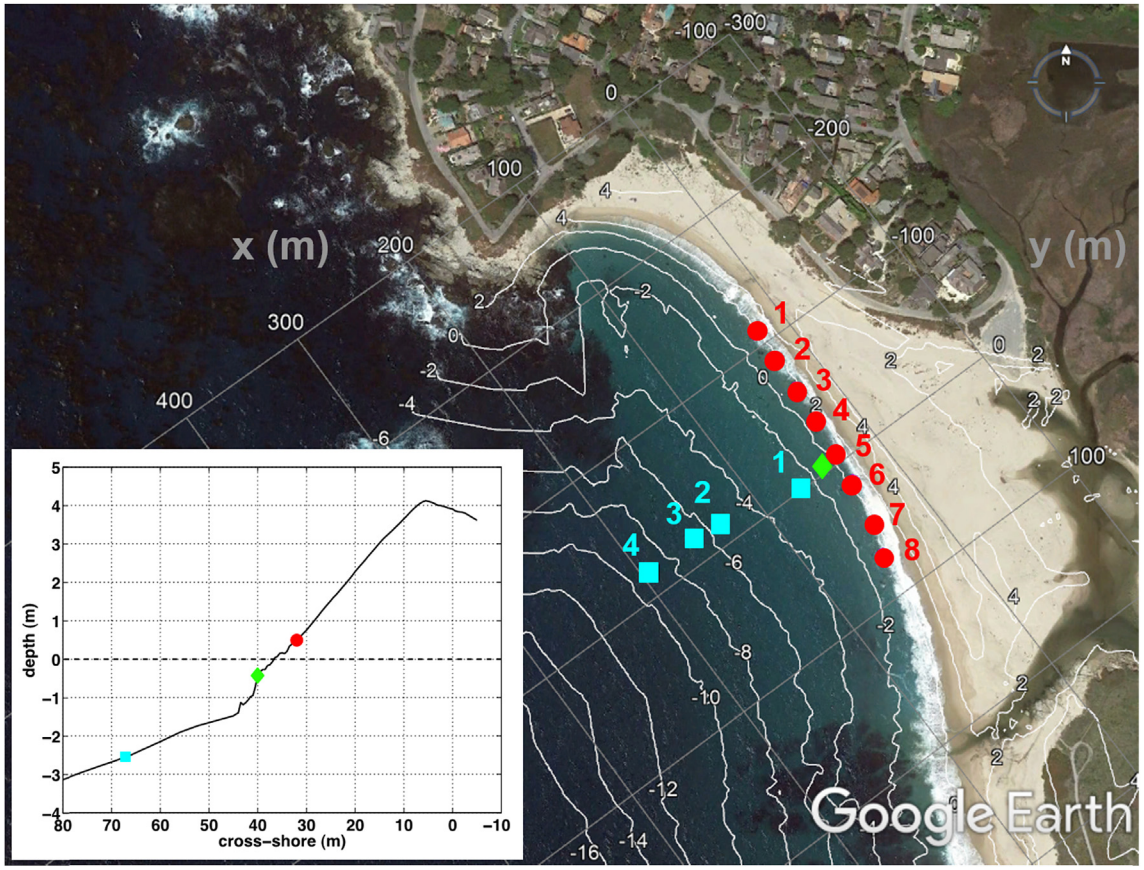

Fig. 1. Carmel River State Beach, California, field site aerial view shown with a Google Earth image and bathymetry contours in meters overlaid in white. The inset shows the mean cross-shore beach profile, relative to mean sea level. Red dots represent the alongshore array of stationary dye sensors, cyan squares represent the cross-shore array of ADCPs, and the green diamond represents the location of the EMCM array. The local coordinate system is shown, where the origin is in the center of the beach, and the cross-shore coordinate x is positive offshore and the alongshore coordinate y is positive to the south. (For interpretation of the references to color in this figure legend, the reader is referred to the Web version of this article.)

surfzone.

2.2. Wave and current measurements

Offshore waves and currents (Fig. 2) were measured with a cross-shore array of four bottom-mounted, upward-looking acoustic Doppler current profilers (ADCPs) and pressure sensors (Fig. 1), sampled at 1 Hz, throughout the experiment. Additionally, a vertical array of six Electro-Magnetic Current Meters (EMCMs) spaced at 0.2 m intervals was deployed in 0.4 m water depth relative to mean sea level (MSL) and sampled at 16 Hz for 5 days (yeardays 169 to 173) to observe the vertical structure of the cross-shore and alongshore currents associated with the steep beach surfzone. Hourly, depth-averaged currents (u_{avg}, v_{avg}) were computed from the ADCPs and EMCM array measurements to evaluate the mean currents inside and outside the surfzone (Fig. 2, rows 3 and 4). The tidal elevation with respect to MSL during the experiment was approximately ± 1 m (Fig. 2, row 5), so that the EMCMs were located inside and outside the region of active wave breaking as a function of tidal elevation and wave energy. Depth-limited wave height decay is defined as $H_b = \gamma_s h$, where h is local depth and $\gamma_s = 0.19 + 1.05\beta(kh)^{-1}$ for steep beaches (Raubenheimer and Guza, 1996), where β is the local beach slope and k is the wavenumber. Using this definition, a local wave breaking criterion of $\gamma_s > 1$ was used to determine when the EMCMs were inside the surfzone, which was typically during low tides. Throughout the experiment, waves approached the field site obliquely from the northwest, resulting in a predominant alongshore current to the south (Fig. 2, row 4).

2.3. Dye experiments

Dye was released on five different days over the course of ten-days during varying wave and alongshore-current conditions (Fig. 2), resulting in 15 successful dye releases. An initial volume of 200 mL of fluorescent Rhodamine dye (20% weight per volume) was released as a slug in the surfzone (Fig. 3a) at mid-depth in the shallow water at the shoreline. Rhodamine dye was chosen since its decay rate is minimal and it is relatively stable in ambient light (Smart and Laidlaw, 1977; Grant et al., 2005). The dye sensors used to measure dye concentration were 1 Hz internal logging WET Labs fluorometers with a 0–230 ppb range. Clark et al., (2009) found that the instantaneous 1 Hz concentration errors were ~1 ppb in a bubbly, sediment suspended surfzone with medium-grained quartz sand and minimal fine sediments. Similar measurement errors are assumed at CRSB, which had coarse sand with minimal fines.

The temporal and spatial distribution of the dye was evaluated with an alongshore array of eight dye sensors with a spacing of approximately 25 m in the alongshore (Fig. 1). The dye sensors were mounted on poles jetted into the sea-bed on the upper beachface (Fig. 3c–f) and were affixed vertically with their optical sensors facing downward approximately 10 cm off the sea-bed, such that they were submerged for the longest duration possible in the surfzone waves. Owing to the fixed location of the stationary dye sensor array, the individual dye studies were performed at approximately the same tidal elevation, about 0.5 m above MSL, such that the dye sensors were located in the active surfzone. The dye was generally released between poles toward the northern end or in the middle of the array owing to the predominant

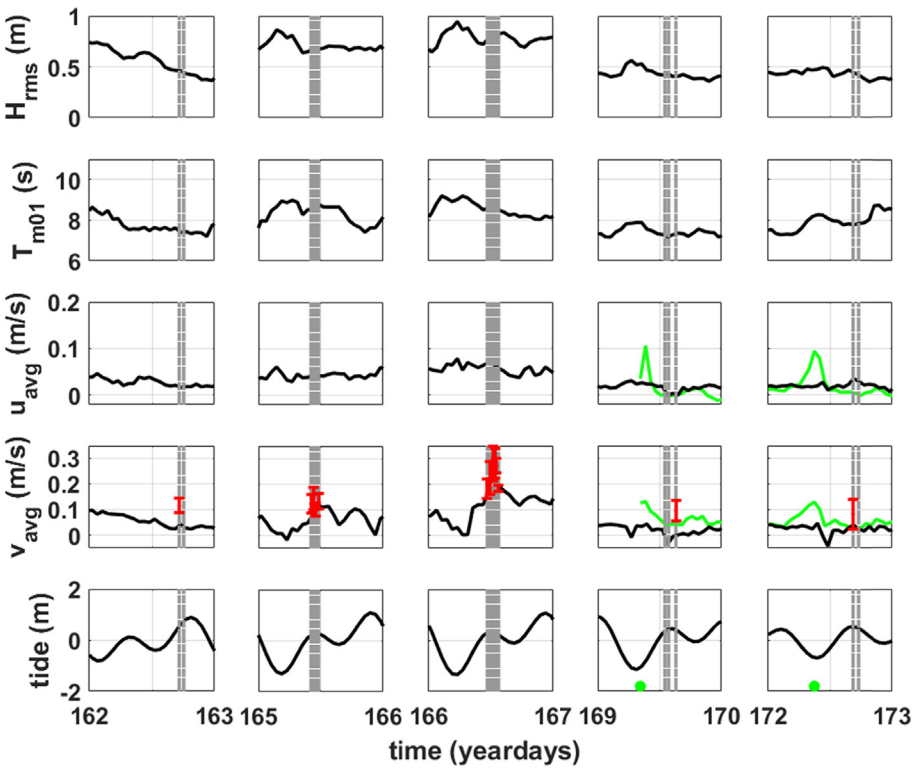

Fig. 2. Hourly-mean (row 1) root-mean square wave height, H_{rms}, (row 2) mean wave period, T_{m01}, (row 3) depth-averaged cross-shore velocity, (row 4) depth-averaged alongshore velocity, and (row 5) tidal elevation measured at ADCP1 in 3 m water depth. Red dots and error bars in row 4 represent surfzone currents estimated with the dye. Green lines in rows 3 and 4 represent depth-averaged velocities measured by the EMCM array in 0.4 m water depth, and green dots in row 5 represent times when the EMCM array was inside the surf zone. Vertical dashed grey lines represent times of dye releases. Velocities are in the local coordinate system where cross-shore velocity u_{avg} is positive offshore and alongshore velocity v_{avg} is positive to the south. (For interpretation of the references to color in this figure legend, the reader is referred to the Web version of this article.)

southward surfzone alongshore current.

The location of the alongshore array in the active surf/swash zone resulted in the dye sensors being alternately submerged and not submerged within the sea-swell water level range, which varied due to tidal elevation and minimal infragravity motions (Fig. 3c and d), resulting in dropouts in measurements of dye concentration. Including these dropouts would bias the measurements toward low concentrations; therefore, to account for this in the measured dye concentration time series, an envelope was fitted to the maxima of concentration peaks associated with the sea-swell waves (Fig. 4) to describe the actual concentration of dye in the surf/swash zone as a function of time. No procedure allowed for 100% automation, so the envelope was manually selected after some initial automation, which also removed erroneous values.

Additionally, during some of the dye releases, swimmers each equipped with a dye sensor and a GPS device performed repeated cross-shore transects from the shoreline to beyond the offshore edge of the dye plume and back in approximately the same alongshore location for the duration of the dye deployment. This resulted in a measure of the dye concentration as a function of cross-shore distance and time, $C(x,t)$. Each swimmer performed 13 to 20 cross-shore transects (out and back) at a given alongshore location during a given dye release, resulting in 26–40 measurements of $C(x,t)$ per swimmer per dye release. As the dye spread offshore, the swimmers had to travel farther, swimming between 5 and 45 m offshore and back, taking on average 2 min to complete a transect.

3. Eulerian current measurements

3.1. Steep beach surf/swash zone cross-shore velocities

The surfzone on the steep beach at CRSB can be described as being a large swash zone. When the EMCM array was inside of the surf/swash zone, the sensors became alternately submerged and not submerged, depending on their location in the water column, with the frequency of the incident waves. A 1-min time series of cross-shore velocity measured by each sensor in the EMCM array when it was inside of the surfzone is shown in Fig. 5a. At times, just prior to and during wave breaking (e.g., $t = 0$ s), there were strong onshore (negative) velocities measured by all sensors in the vertical array. As the flow switched direction, the sensors nearest to the water surface (≥ 0.63 m above the sea-bed) immediately became dry and did not measure backwash (positive) velocities. The sensor 0.43 m above the sea-bed (red lines in Fig. 5) measured part of the backwash then became dry, resulting in a velocity measurement of zero. Only the bottom-most sensors (0.03 and 0.23 m above the sea-bed, blue and green lines in Fig. 5) measured offshore velocities throughout the entire backwash (Fig. 5a). Although the EMCM array was in a mean water depth of 0.7 m during this example time series, the measured velocities still exhibit swash zone velocity characteristics. When the EMCM array was outside of the surf/swash zone, all of the sensors in the vertical array were submerged and measured velocities at all times (Fig. 5b).

3.2. Undertow inside and outside surfzone

The vertical structure of the cross-shore flow inside and outside of the surfzone was evaluated using half-hour averaged EMCM and ADCP1 velocity measurements (Fig. 6). When the EMCM array was inside the surfzone, an undertow profile was observed, with the characteristic parabolic shape and maximum offshore velocity at mid-depth, which is typically observed within the surfzone on alongshore-homogeneous dissipative beaches (Garcez Faria et al., 2000; Reniers et al., 2004). The undertow velocity changed from a small offshore velocity throughout the water column when the EMCM array was outside of the surfzone (Fig. 6b, solid circle, square, and triangle symbols) to a strong offshore flow at mid-depth as the EMCM array transitioned to being inside of the surfzone (Fig. 6b, solid star and diamond symbols). This demonstrates that the undertow within the surfzone on this steep, reflective beach was not destroyed by standing waves, which are common on steep beaches (Wright, 1982). The mean measured alongshore velocity was also greatest when the EMCM array was inside the surfzone (Fig. 6c, solid star and diamond symbols).

Fig. 3. Photos showing examples of (a) the initial dye slug release, (b) the well-mixed surf/swash zone shortly after the dye release, (c–d) turbulence and mixing of dye at the shoreline by breaking waves and alongshore advection of dye within the surfzone, and (e–f) run-down colliding with an incoming breaking wave resulting in the dye seeping offshore. Black arrows indicate locations of poles with dye sensors attached near the sea-bed in the surf zone, where (c–d) the intermittency of the dye observations is highlighted as the sensor is alternately submerged and not submerged.

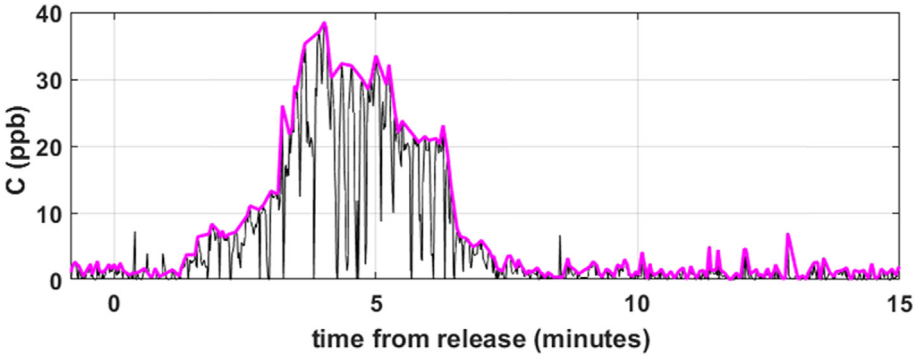

Fig. 4. Example of measured dye concentration as a function of time (black) and the dye envelope fit to the measurements (magenta).

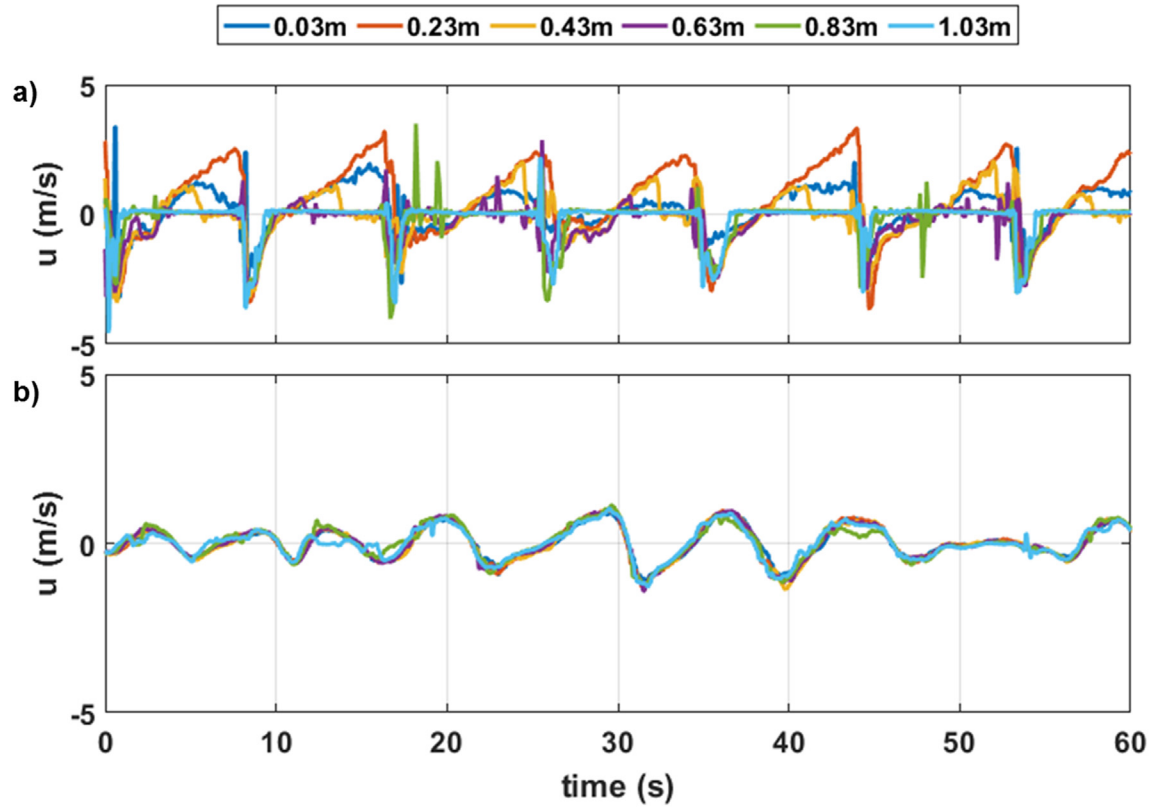

Fig. 5. Example of cross-shore velocities measured by the EMCM array for times when the EMCM array was (top) inside the surf zone and (bottom) outside the surf zone. Cross-shore velocity is in the local coordinate system where positive is offshore. The height of each EMCM sensor above the sea-bed is given in the legend.

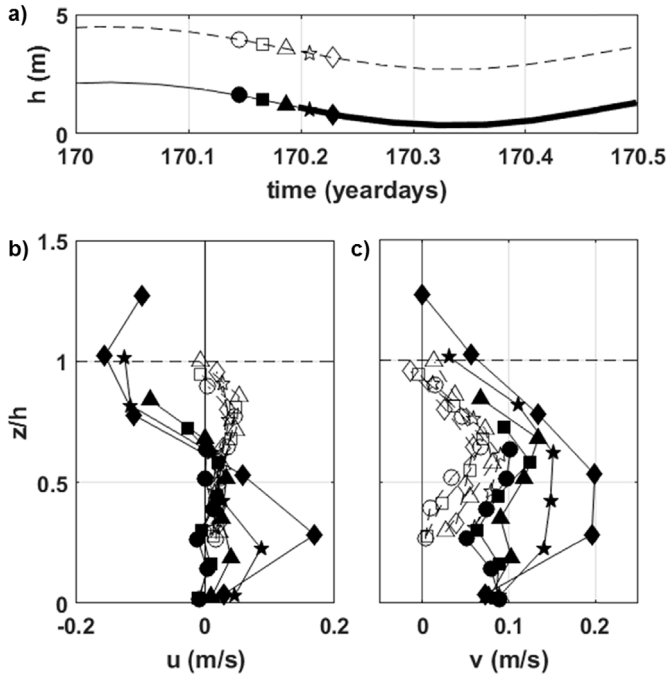

Fig. 6. (a) Water depth measured at ADCP1 (dashed line) and at EMCM array (solid line), with times when the EMCM array was inside of the surf zone shown by the thick black line, (b) half-hour mean cross-shore velocity profiles measured by ADCP1 (open symbols) and EMCM array (solid symbols), and (c) half-hour mean alongshore velocity profiles measured by ADCP1 (open symbols) and EMCM array (solid symbols), as a function of depth-normalized height above the sea-bed. Symbols in the velocity profiles correspond to times in the water depth time series. Velocities are in the local coordinate system where positive is offshore and to the south.

Outside of the surfzone at ADCP1, located in 3 m water depth approximately 35 m from the shoreline, an undertow profile was also observed, which had maximum offshore flow near the surface and decreased with depth (Fig. 6b, open symbols), consistent with undertow profiles measured on the inner shelf by Lentz et al., (2008). The magnitude of the undertow profile at ADCP1 was similar to that measured with the EMCM array when it was outside the surfzone for corresponding times; the magnitude of the alongshore velocity at ADCP1 was less than that measured by the EMCM array for corresponding times (Fig. 6c). These results indicate that outside of the surfzone there was a decrease in velocity with increasing water depth.

4. Dye measurements

4.1. Qualitative dye observations

The dye was visually observed to mix rapidly throughout the water column and in the cross-shore immediately after the release (Fig. 3a and b), and began to seep offshore of the surfzone shortly thereafter. The predominant pattern observed during the experiment consisted of the dye moving alongshore to the south, while also slowly being transported offshore. When the alongshore current was weak, the offshore movement of the dye was more visually noticeable because it stayed at approximately the same alongshore location, however it was found to move offshore at the same slow rate as when the alongshore current was strong. A summary of the visual dye patterns is given in Table 1.

The movement of the dye was examined with the dye concentration time series, $C(t)$, measured at each alongshore sensor (Fig. 7). Unfortunately, there were times when the dye concentration was greater than the maximum limit of a dye sensor and the data were clipped, or some sensors were lost or removed when dye was still in the study area, so a complete dye mass balance could not be performed and observations from these dye releases are not discussed. Repeated cross-shore

Table 1
Description of the dye releases and observations, and the sensors used to estimate mixing and transport. Surfzone-averaged alongshore current $\bar{V}$ is equal to the alongshore-mean $V(y)$ computed using Equation (5).

Release	Dye Release Location (between poles)	Visual Dye Observations	Sensors Used for Flux Calculations	$\bar{V}$ (m s^{-1})
162a	3 & 4	predominantly offshore	1–8	0.11 ± 0.03
165a	3 & 4	predominantly alongshore	1-6, 8	0.12 ± 0.01
165b	1 & 2	predominantly alongshore	1, 3–6, 8	0.14 ± 0.02
165c	1 & 2	predominantly alongshore	1, 3–6, 8	0.10 ± 0.01
165d	1 & 2	predominantly alongshore	1, 3-6	0.13 ± 0.02
166a	1 & 2	predominantly alongshore	1, 3–6, 8	0.18 ± 0.03
166b	1 & 2	predominantly alongshore	1, 3–6, 8	0.19 ± 0.04
166c	1 & 2	predominantly alongshore	1, 3–6, 8	0.29 ± 0.05
166d	2 & 3	predominantly alongshore	1, 4–6, 8	0.22 ± 0.05
166e	2 & 3	predominantly alongshore	1, 3–6, 8	0.26 ± 0.03
166f	2 & 3	predominantly alongshore	1, 3–6, 8	0.19 ± 0.02
169b	5 & 6	predominantly offshore	3 swimmers	
169c	4 & 5	offshore and alongshore	4–8	0.09 ± 0.07
172a	4.5 & 5	predominantly offshore	4.5–8, 3 swimmers	0.08 ± 0.01
172b	4.5 & 5	predominantly offshore	2 swimmers	

transects performed by swimmers during some of the dye releases also provide a measure of the offshore movement of the dye plume. The dye sensors in the alongshore array and/or the swimmers that were used to compute mass transport estimates during each dye release are given in Table 1.

The dye releases on yeardays 162, 169 and 172 occurred during relatively small offshore wave conditions (H_{rms} < 0.5 m at ADCP1), which forced relatively weak alongshore currents (v_{avg} < 0.1 m/s at ADCP1), and the dye visually appeared to move primarily offshore. During the dye releases on these yeardays, two distinct peaks in $C(t)$ were measured by the dye sensor nearest to the dye release, indicating a separation in the dye (example shown in Fig. 7a of dye release 162a). The dye initially reached the sensor nearest to the dye release location and moved offshore, seen by a narrow peak and sharp decrease in $C(t)$. Then the remaining dye reached the sensor and gradually moved offshore, seen by a second, broader peak in $C(t)$ measured by the same sensor. The $C(t)$ measured by the subsequent sensors to the south in the alongshore array show broader profiles with smaller peak concentrations, indicating that the dye continued to spread alongshore and travel downstream, which can also be seen in the time evolution of $C(y)$ (Fig. 7b). These measurements were consistent with visual observations. Due to the weak alongshore current and reduced number of stationary dye sensors that measured concentration time series, quantitative estimates using the alongshore array of stationary sensors were limited. Cross-shore profiles of dye concentration measured by the swimmers on yeardays 169 and 172 were used to examine the cross-

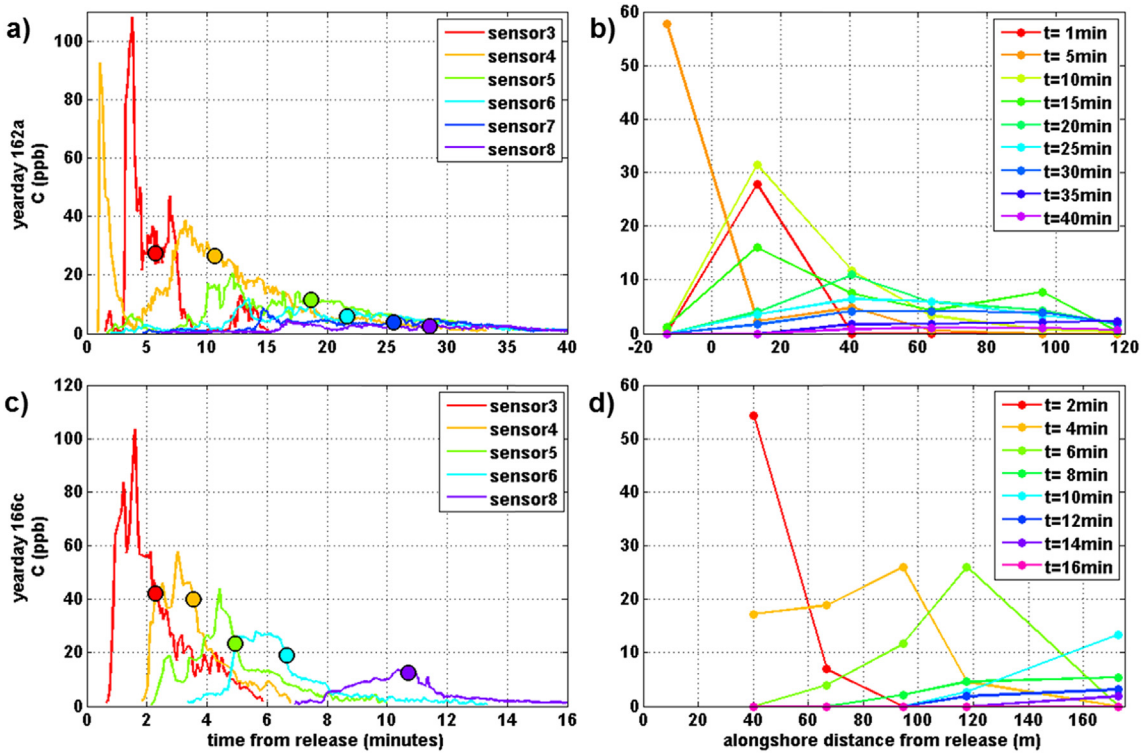

Fig. 7. Dye concentration as a function of (left) time and (right) alongshore distance from the dye release measured by the alongshore array of stationary dye sensors for (a, b) yearday 162a during weak alongshore current conditions, and (c, d) yearday 166c during strong alongshore current conditions. In the left plots, colored circles represent the first moment of the dye concentration time series, t_{m01}, computed with Equation (1). In the right plots, the dye was released at $y = 0$, and the dots represent the alongshore locations of the dye sensors.

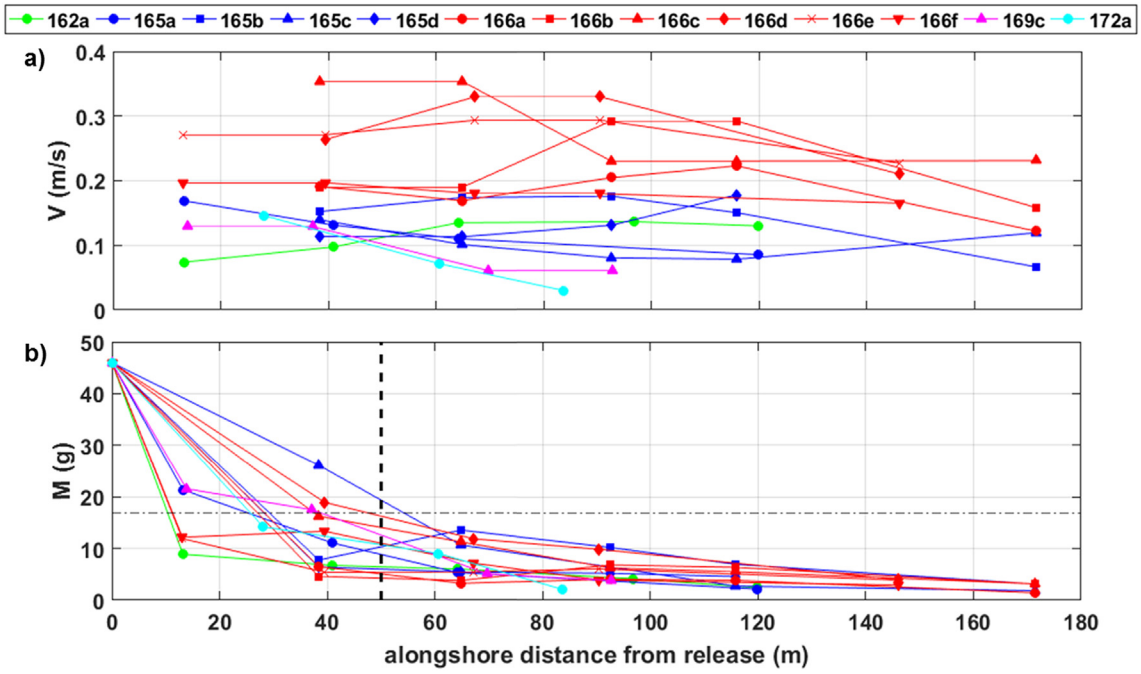

Fig. 8. Estimates based on the dye concentration time series measured by the alongshore stationary dye sensor array of (a) the surfzone averaged alongshore current V using Equation (5), and (b) the alongshore decay of dye mass $M(y)$ using Equation (6). In (b) the horizontal black dashed-dotted line represents where M_0 decreases by $1/e$, and the vertical black dashed lines represent the division between the near-field and far-field regions of transport.

shore movement of the dye.

The dye releases on yeardays 165 and 166 occurred during relatively larger offshore wave conditions ($H_{rms} > 0.5$ m at ADCP1), which forced relatively strong alongshore currents ($v_{avg} > 0.1$ m/s at ADCP1). The dye was released at the northern end of the array and appeared to move quickly alongshore to the south inside the surfzone with slight cross-shore movement (example shown in Fig. 7c of dye release 166c). The $C(t)$ measured at the sensor nearest to the dye release showed a sharp rise followed by a rapid decay resulting in a relatively narrow concentration peak. As the dye reached the subsequent downstream alongshore sensors, the rise in concentration was less steep and it decayed more slowly, resulting in a broader concentration peak. The measured peak concentration moved quickly alongshore, and also decreased with alongshore distance from the dye release, as seen in the time evolution of $C(y)$ (Fig. 7d). There were no traces of dye measured by the sensors after 35 min during these releases. Swimmer data could not be used to examine the cross-shore movement of dye during these releases because the dye moved too quickly past the locations of the swimmer transects and was not adequately captured.

4.2. Quantitative dye statistics

The statistical moments of the dye concentration, in both time and space, are used to describe the dye distributions measured with the alongshore dye sensor array and cross-shore swimmer transects. The weighted-mean time of a dye concentration time series at each dye sensor location can be described by the first moment as

$$t_{m01}(x_i) = \frac{\int_0^T tC(x_i, t)dt}{\int_0^T C(x_i, t)dt}, \quad i = x, y, \tag{1}$$

where $C(x_i,t)$ is the dye concentration as a function of direction, $i = x, y$, and time, t, from the dye release ($x = 0$, $y = 0$, $t = 0$) and T is the duration of the dye measurements. Similarly, the dye center of mass, μ, is given by the first moment of each dye concentration profile,

$$\mu_i(t) = \frac{\int x_i C(x_i, t)dx_i}{\int C(x_i, t)dx_i}, \quad i = x, y \tag{2}$$

and the variance, σ^2, is given as the second moment of the concentration profile,

$$\sigma_i^2(t) = \frac{\int [x_i - \mu_i]^2 C(x_i, t)dx_i}{\int C(x_i, t)dx_i}, \quad i = x, y, \tag{3}$$

and the limits of integration depend on the given direction (Clark et al., 2010). The rate of spreading of the dye is described by the diffusivity, κ, which is computed as the time rate of change of the variance,

$$\kappa_i(t) = \frac{1}{2}\frac{d\sigma_i^2}{dt}, \quad i = x, y. \tag{4}$$

4.3. Alongshore mixing and transport inside surfzone

4.3.1. Surfzone-averaged alongshore current

In-situ surfzone velocity measurements were not obtained during most of the dye releases. Therefore, a Eulerian measure of the alongshore current inside the surfzone was estimated as the velocity, V, that the dye was advected alongshore past each instrument. The dye concentration time series measured with the alongshore array of stationary dye sensors were used and assumed to represent the surfzone-averaged concentration. The alongshore velocity was calculated by

$$V(y) = \frac{y}{t_{m01}(y)}, \tag{5}$$

where y is the linear distance of the sensor from the dye release and $t_{m01}(y)$ is the time of arrival of the first moment of the dye concentration time series calculated using Equation (1) for $i = y$ (e.g. Fig. 7). Due to separations in the dye patch as it moved alongshore, it was found that t_{m01}, which represents the weighted-mean concentration time associated with the dye profile, provided a better estimate of $V(y)$ rather than using the time associated with the leading edge of the dye plume, the time associated with peak dye concentration, or the time associated with the trailing 10% of the peak dye concentration. The effect of

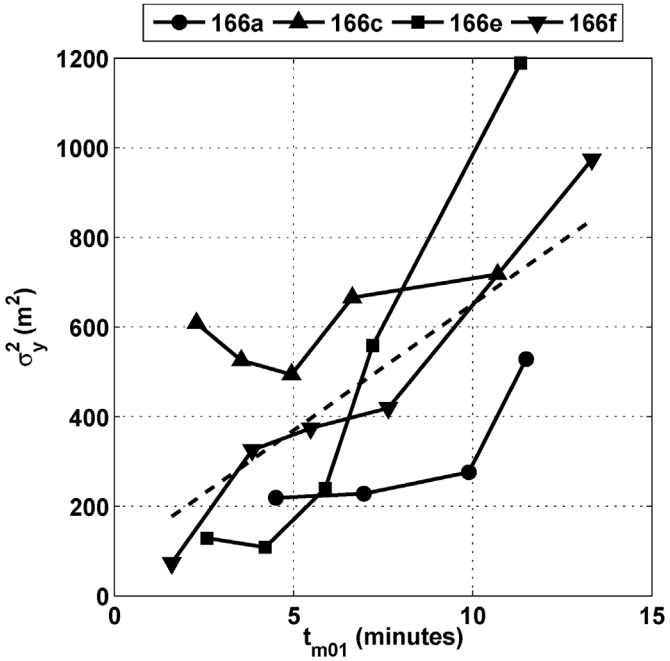

Fig. 9. Dye dispersion inside of the surf zone measured with the alongshore array of stationary sensors as a function of weight-mean concentration time t_{m01}. The dashed line represents the line of best-fit for all measurements on yearday 166, which has an $r^2 = 0.44$ and is significant in the 95% confidence interval. The alongshore diffusivity κ_y is equal to half of the slope of the best-fit line.

alongshore diffusion on the estimates of t_{m01} are assumed negligible in the $V(y)$ calculations.

The alongshore current $V(y)$ is determined at each alongshore instrument location (Fig. 8a), where $V(y)$ represents a surfzone-averaged alongshore current since the dye is mixed evenly across the surfzone. Errors in the estimates of $V(y)$ were determined based on the maximum and minimum possible differences in time of dye arrival between alongshore sensors, where the ranges in time were computed as the upper and lower limits of the 95% confidence intervals on t_{m01}. Estimates of $V(y)$ tended to decrease slightly with distance alongshore (Fig. 8a), with alongshore averages computed over the length of measurements, $\bar{V}$, ranged from 0.1 to 0.3 m/s for all dye releases with a mean error of ± 0.03 m/s (Table 1). The decrease in $V(y)$ with distance alongshore to the south could be due to the dynamics associated with the curvature of CRSB and is discussed in Section 5.2.

The estimates of $\bar{V}$ from the dye inside the surfzone are compared with the depth-averaged Eulerian velocities measured by the EMCM array and ADCP1 (Fig. 2, row 4). Estimates of $\bar{V}$ from the dye are consistent with the alongshore velocities measured by the EMCM array when it was inside of the surfzone (Fig. 2, row 4, green), which typically occurred during low tides; unfortunately, a direct comparison could not be made because the EMCM array was never inside the surfzone during the dye releases. The dye estimates of $\bar{V}$ inside the surfzone were faster than the depth-averaged alongshore velocities measured outside the surfzone by ADCP1 (Fig. 2, row 4, black) and by the EMCM array when it was outside the surfzone (Fig. 2, row 4, green), which typically occurred during high tides.

4.3.2. Alongshore mass transport

Comparisons of the mass of dye measured at each subsequent alongshore sensor during a dye release describe the alongshore advection and dispersion of the dye, and any loss of dye between alongshore sensors is attributed to cross-shore exchange. Assuming an alongshore uniform cross-sectional surfzone area, and that the dye is well-mixed (throughout the water column and in the cross-shore) and is moving with the alongshore-averaged, surfzone-averaged, alongshore current $\bar{V}$, the total mass of dye advected past each alongshore dye sensor, $M(y)$, measured in grams (1 ppb = 10^{-3} g m^{-3}) was estimated by

$$M(y) = \int_0^T A_c \bar{V} C(y, t) dt, \tag{6}$$

where A_c is the cross-sectional area of the surfzone, which was considered to be a wedge, and was computed as $A_c = 0.5 h_b x_w$, where $h_b = 1$ m and is the water depth at the offshore edge of the surfzone, and $x_w = 10$ m is the approximate surfzone width. The initial amount of dye released in the surfzone, $M(y = 0)$, was $M_0 = 46$ g. The mass transport measured as a function of alongshore distance from the dye release was computed using estimates of $\bar{V}$ (Fig. 8b). Errors in the estimates of $M(y)$ were generally within ± 2 g, based on the range in estimates of $V(y)$ determined at each alongshore sensor. The $M(y)$ decreased by a value of $1/e$ within 10–50 m from the dye release location, with a more gradual decrease in dye mass measured with increasing distance alongshore thereafter.

The statistical significance of the alongshore decay of $M(y)$ was examined by evaluating the mean dye concentration, $\bar{C}$, measured at each dye sensor in the alongshore array for each dye release, where $\int_0^T C(y, t) dt = T\bar{C}$. Then, $M_{meas}(y) = A_c \bar{V} T \bar{C}$ and the statistics associated with $\bar{C}$ can be applied to $M(y)$. Confidence intervals were estimated for $\bar{C}$, and the decay with distance alongshore was found to be statistically significant at the 95% confidence level (not shown), which is used to demonstrate the statistical significance in the decay of dye mass $M(y)$ with distance alongshore.

4.3.3. Alongshore diffusivity

The alongshore spreading of the dye inside the surfzone from a narrow peak to a broad profile over a short alongshore distance (< 100 m) as a function of time (Fig. 7) is described by the alongshore diffusivity, κ_y. Equations (2)–(4) are evaluated for $i = y$, using $C(y,t)$ measured by the alongshore array and integrating over the length of the alongshore array. Multiple dye releases were made over a 2-h period on yearday 166. During this time, the waves were near stationary with little depth variation over the peak of a lower high tide (Fig. 2). These results were ensemble averaged and used to characterize the alongshore diffusivity at CRSB. Linear regression of σ_y^2 versus t_{m01} (Fig. 9) is used to fit a line to the data from all dye releases on yearday 166 ($r^2 = 0.44$, significant in the 95% confidence interval), where half of the slope of the line represents κ_y (Equation (4)). Values of κ_y varied for the individual deployments. The mean κ_y inside of the surfzone was found to be 0.5 m^2 s^{-1}, which is less than values found on dissipative beaches.

4.4. Cross-shore mixing

The cross-shore movement of the dye was estimated using cross-shore dye concentration profiles measured by swimmers on yeardays 169b and 172a,b (Table 1; Fig. 10, upper panels). To summarize the offshore movement of dye, the swimmer concentration profiles (26–40 per deployment, per swimmer) were averaged over 5-min time windows to obtain mean concentration profiles as a function of cross-shore distance (Fig. 10, lower panels). The cross-shore location of the dye plume, $\mu_x(t)$, was found at each alongshore swimmer transect location for each 5-min mean $C(x,t)$ measured by the swimmer using Equation (2) with $i = x$, where the limits of integration were from the shoreline to beyond the offshore extent of the dye plume ($x = 80$ m).

The cross-shore dye concentration profiles at each alongshore location show the dye was initially shoreline-attached and saturated the surfzone in less than 5 min. The measured dye concentration decreased with time, and μ_x moved offshore as the dye concentration profile spread in the cross-shore. Due to the presence of the shoreline, μ_x is expected to move offshore as the dye disperses in the cross-shore,

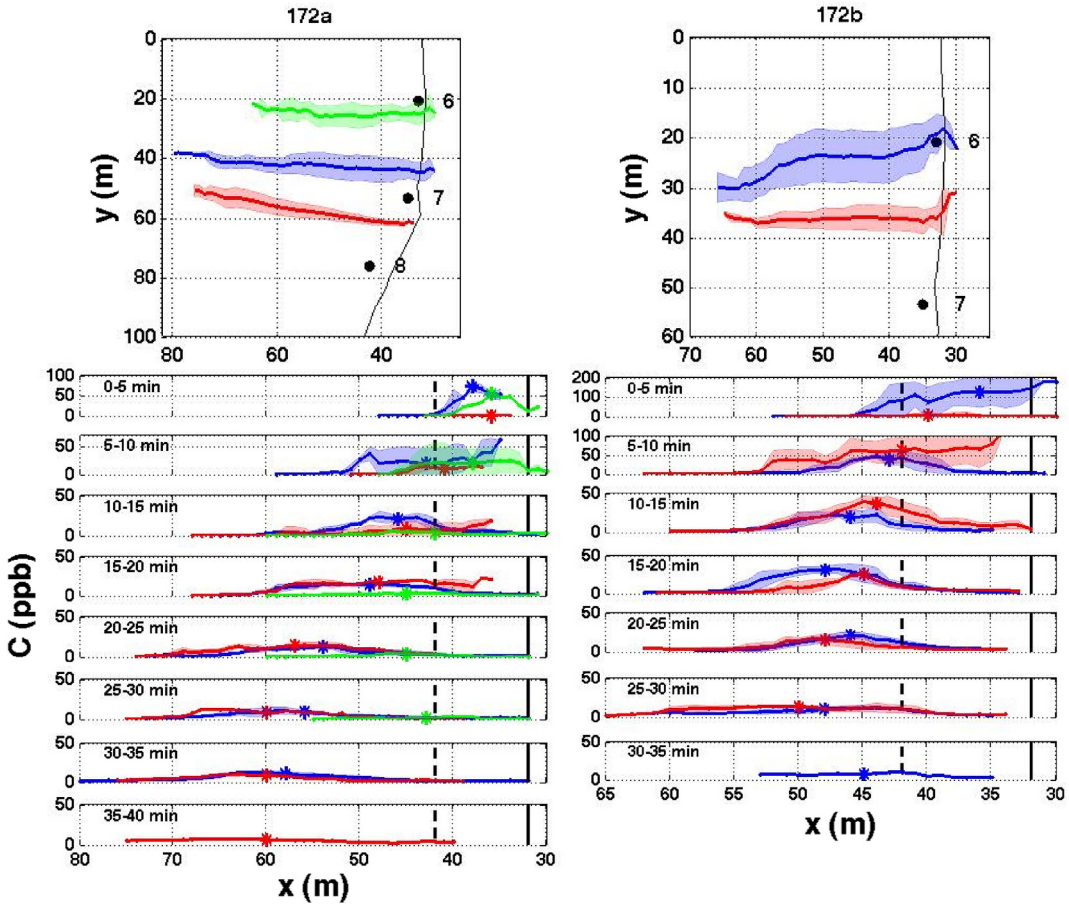

Fig. 10. Example of data collected by swimmers for dye releases (left) 172a and (right) 172b. Multiple swimmers performed (top) repeated cross-shore transects at different alongshore locations, where the black dots and corresponding number refer to dye sensors, and (bottom) the corresponding mean dye concentration profiles as a function of cross-shore distance for 5-min time windows are shown. Each color represents a different swimmer, and solid lines represent their mean cross-shore transect with ± one standard deviation represented by shaded areas. In the bottom plots, solid vertical black lines represent the approximate location of the shoreline, dashed vertical black lines represent the approximate edge of surf zone, and asterisks indicate the first moment of the dye concentration profile representing the cross-shore location of the dye plume μ_x. The local coordinate system is used where the cross-shore coordinate x is positive offshore and the alongshore coordinate y is positive to the south. (For interpretation of the references to color in this figure legend, the reader is referred to the Web version of this article.)

however this could be due to seaward advection and/or plume widening by cross-shore diffusion (Clark et al., 2010; Spydell and Feddersen, 2012). Unlike the shoreline-attached cross-shore concentration profiles and offshore μ_x movement with increasing alongshore distance from the dye source observed by Clark et al., (2010), which was attributed to cross-shore plume widening, the cross-shore concentration profiles observed at CRSB showed the peak concentration moving offshore as well as μ_x, indicating the dye was being advected offshore as well as being spread by cross-shore diffusion.

The μ_x moved outside the surfzone after 10 min but remained within 20 m (2 surfzone widths) of the edge of the surfzone, indicating a decrease in the cross-shore dispersion of the dye outside the surfzone. The maximum cross-shore extent of measured dye ranged from 1.9 to 3.8 surfzone widths beyond the surfzone boundary for all alongshore swimmer locations. The cross-shore extent measured with surface drifters of 1 to 2 surfzone widths beyond the surfzone boundary for a rip-channeled beach (Brown et al., 2015) corresponded to smaller diffusivities and less lateral shear in the flow outside the surfzone. In numerical simulations of cross-shore exchange on an alongshore uniform beach using a wave-resolving model and considering unstratified and stratified inner shelf regions, results suggest that stratification and the presence of transient rip currents results in a greater amount of cross-shore exchange, with transport up to 3 surfzone widths beyond the surfzone boundary (Kumar and Feddersen, 2017a; 2017b), which is scalable with beach slope and incident wave conditions (Suanda and Feddersen, 2015). In this work, a greater cross-shore extent was measured, however inner shelf stratification measurements were not obtained and the influence on the mixing and cross-shore extent of transport outside the surfzone on this steep beach could not be evaluated.

4.4.1. Cross-shore diffusivity inside surfzone

The cross-shore spreading of the dye within the surfzone was not accurately captured with the swimmer transects, as they were performed a considerable distance (> 50 m) downstream of the dye release, and due to the steepness of the beach and the narrowness of the surfzone, the dye plume had already spread across the surfzone and moved offshore. The observed rapid cross-shore mixing in the shallow surf/swash zone during the dye releases indicates the cross-shore diffusivity inside of the surfzone is due to breaking wave-induced turbulence generated by the intense breaking of plunging/surging waves near the shoreline on this steep beach. Feddersen (2012) derived a surfzone turbulent dissipation rate scaling assuming weak mean currents and a vertically uniform length-scale, resulting in a non-dimensional surfzone eddy diffusivity coefficient, K. The scaling is based on a balance between vertical turbulent diffusion and energy dissipation, analogous to work by Battjes (1975), however a vertically-uniform length-scale equal to a fraction, λ, of the mean water depth, h, is used, which is representative of small-scale turbulent eddies. The non-dimensional eddy diffusivity K as a function of height about the sea-bed,

z, is

$$\frac{K(z)}{h(\varepsilon_b/\rho)^{1/3}} = \lambda^{4/3}B^{1/3}\exp\left(\frac{\alpha}{3}\frac{z}{h}\right), \quad (7)$$

where ε_b is the total wave energy dissipated across the surfzone, ρ is the density of seawater, and $B = \alpha/\exp(\alpha)$, where $\alpha = (3/2)^{1/2}C_\mu/\lambda$ and $C_\mu = 0.57$ (Feddersen, 2012). The dissipation of incident wave energy by breaking waves within the surfzone ε_b is estimated based on the cross-shore conservation of wave energy flux (Battjes, 1975), assuming straight and parallel contours. Energy flux is conserved up to wave breaking outside the surfzone, so measurements made by ADCP1 in 3 m water depth are used to describe the wave energy flux at the edge of the surfzone, $x = x_w$. Integrating across the surfzone and assuming the wave energy flux at the shoreline, $x = 0$, equal to zero, dissipation is equal to the energy flux measured by ADCP1. To account for the reflective nature of the steep beach, the incident wave energy flux is multiplied by a factor of $(1 - R^2)$, where R^2 is the reflection coefficient. Hence, the total surfzone wave energy dissipation is found by

$$\varepsilon_b = \frac{(Ec_{gx})_{ADCP1}(1 - R^2)}{x_w}, \quad (8)$$

where $E = {}^1/_{16}\rho g H_s^2$ is the wave energy, with g being the acceleration due to gravity and H_s being significant wave height, c_{gx} is the wave group velocity in the cross-shore direction determined using linear wave theory (Battjes, 1975), and $R^2 = 0.4$ is the reflection coefficient for CRSB computed using the energy flux method by Sheremet et al., (2002). Owing to the surfzone at CRSB effectively being a large swash zone, the h used in Equation (7) was set equal to the wave height H_s measured at ADCP1, and the turbulent length-scale was assumed equal to the entire water column ($\lambda = 1$). Values of the depth-averaged $K(z)$ are assumed equal to the cross-shore turbulent eddy diffusivity κ_x inside of the surfzone, with values ranging from 0.2 to 0.5 $m^2\,s^{-1}$ for the times of the dye releases. Estimates of κ_x inside of the surfzone are the same order of magnitude as κ_y found inside of the surfzone and are smaller than asymptotic surfzone κ_x measured on dissipative beaches using drifters (Spydell et al., 2007; Brown et al., 2009) and dye (Clark et al., 2010).

4.4.2. Cross-shore diffusivity outside surfzone

The spreading of the dye outside the surfzone is expected to be slower than the initial rapid cross-shore mixing inside the surfzone due to the lack of turbulence (Harris et al., 1963; Inman et al., 1971; Clark et al., 2010), and therefore is assumed to behave independently from the processes inside the surfzone. In order to examine the spreading of the dye outside the surfzone using the swimmer transects during dye releases 169b, 172a, and 172b, the total area under $C(x,t)$ was calculated (C_{tot}), as well as the area under $C(x_{out},t)$ corresponding to the portion of the dye concentration profile outside the surfzone, $x_{out} > x_w$ (C_{out}). A ratio of $C_{out}/C_{tot} > 85\%$ was used to conservatively determine when swimmer transects were predominantly outside the surfzone, and only these transects were used here. The cross-shore diffusivity, κ_x, seaward of the surfzone was calculated using Equations (2)–(4) for $i = x$, and integrating $C(x,t)$ from the shoreline to the seaward limit of the seaward transects and vice versa for the shoreward transects. Estimates of cross-shore diffusivity outside the surfzone were found using linear regression of ${\sigma_x}^2$ versus t_{m01} (Fig. 11), where half of the slope of the line represents κ_x (Equation (4)). The correlation coefficients, r, were computed and those that were significant at the 95% confidence level were used. Values of κ_x outside of the surfzone ranged from 0.004 to 0.017 m^2/s with a mean of 0.01 m^2/s. Estimates of κ_x outside of the surfzone are 20–50 times smaller than that inside of the surfzone. These results are consistent with previous findings for dissipative beaches (Fong and Stacey, 2003; Clark et al., 2010; Brown et al., 2015), which suggest that the processes outside of the surfzone are disconnected from the surfzone dispersion processes, however the cross-shore diffusivity measured outside the surfzone on this steep beach are nearly an order of magnitude less than values measured on the inner shelf of alongshore uniform (Fong and Stacey, 2003; Spydell et al., 2007) and rip-channeled (Brown et al., 2009; Brown et al., 2015) dissipative beaches.

5. Discussion

5.1. Stages of mixing and transport inside surfzone on a steep beach

The dye observations at CRSB show differences in the decay of $M(y)$ within the region approximately $y < 10$–50 m of the dye release and the region farther downstream alongshore (Fig. 8), indicating two separate stages of mixing and transport are apparent inside the surfzone on the steep beach (Fig. 12). These observations are analogous to the stages of mixing in rivers (Fischer et al., 1979). In the near-field, a tracer discharged into a river channel initially mixes in three dimensions until vertically well-mixed, then continues to mix horizontally primarily by turbulence as it is advected downstream by the mean current, until fully mixed across the channel. Downstream of this region is considered the far-field where longitudinal shear flow dispersion is the dominant mixing process.

In the surfzone at CRSB, which can be considered a channel with boundaries at the shoreline and offshore edge of the surfzone, the near-field is defined as the region between the dye release and the location downstream where the dye was completely mixed vertically and across the narrow surfzone. The far-field is defined as the region downstream of this point, where the dye is fully mixed. The alongshore location distinguishing the two separate regions is determined using results from dye release 172a when dye concentration measurements are available both in the alongshore and the cross-shore. The dye appears completely mixed across the surfzone after 5 min following the release (Fig. 10) and is assumed to be vertically-mixed since the surfzone is approximately 10 times wider than it is deep. This corresponds to an alongshore distance of approximately 25 m from the dye release location, using $\bar{V} = 0.08$ m/s measured during dye release 172a, and is also where $M(y)$ decreased by a value of $1/e$ (Fig. 8b). Therefore, at CRSB the near-field region is conservatively defined as $0 < y < 50$ m, and the far-field region is $y > 50$ m.

5.1.1. Near-field mixing and transport

In the near-field region of the surfzone, the dye was rapidly mixed throughout the water column immediately after the dye release, and experienced 2-D horizontal mixing and transport until the surfzone was saturated for $y < 50$ m (Fig. 12). The dye was mixed in the cross-shore (κ_x) by turbulence due to breaking waves and spread in the alongshore (κ_y), and was advected alongshore with the surfzone-averaged alongshore current ($\bar{V}$). Observations of $M(y)$ show a decrease by a value of $1/e$ within $y < 50$ m. The strong decay in $M(y)$ suggests that cross-shore diffusion is an important process in controlling the initial 2-D mixing and transport on this steep beach. On shallow sloping dissipative beaches with wide surfzones, suggested mechanisms for mixing in the surfzone are shear instabilities of the alongshore current with scales of order the width of the surfzone and horizontal rotational velocities generated by finite-crest-length wave breaking with scales of order the depth of water (Clark et al., 2010). On this steep beach, where the swash zone constituted the entire surfzone, only the latter mechanisms would be probable. In summary, the Lagrangian surfzone mass transport in the near-field region on this steep beach is due to alongshore advection, longitudinal dispersion and cross-shore diffusion (Fig. 12).

The large decrease in $M(y)$ in the near-field is attributed to the mixing not being steady-state and represents the cross-shore exchange of the dye. The mechanism that initially transports the dye across the breaker line to the offshore is not well understood. On a beach with straight and parallel contours, the local net Eulerian and Lagrangian cross-shore transport is expected to be zero, resulting in no dye being

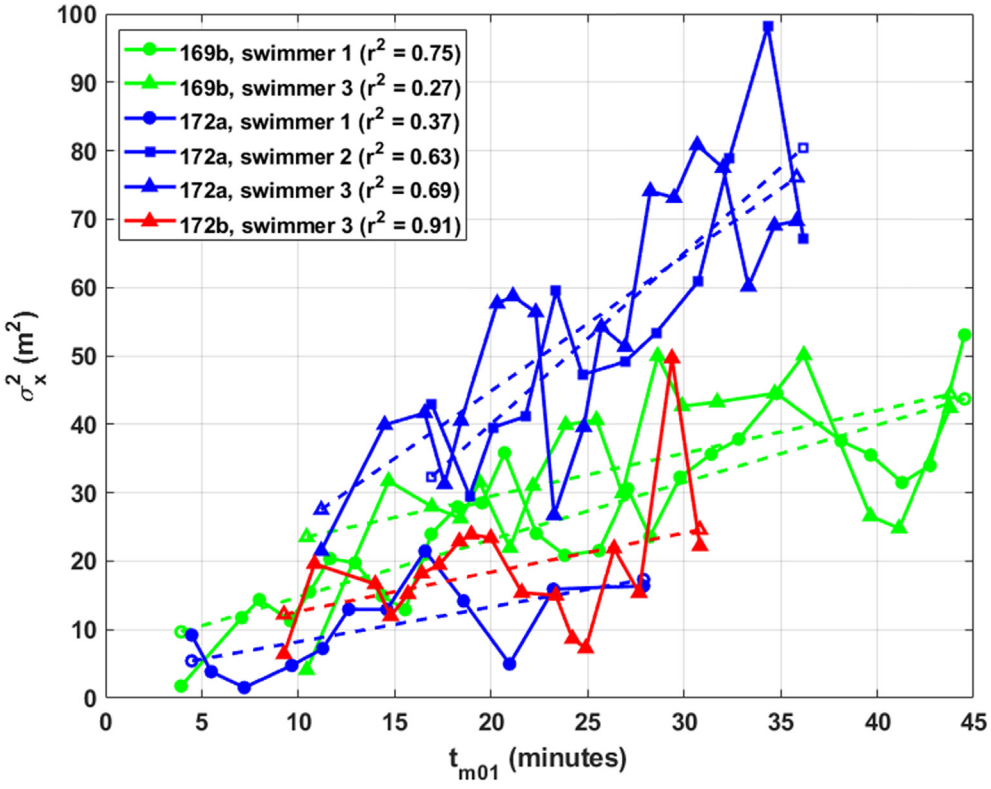

Fig. 11. Dye dispersion outside the surf zone measured with the cross-shore swimmer transects as a function of weighted-mean concentration time t_{m01}. Solid lines of each color represent the dispersion estimates from the swimmer data for that dye release. Dashed lines of each color represent the lines of best-fit for the swimmer data for that dye release. Coefficients of determination are given for each swimmer, with all being significant in the 95% confidence interval. The cross-shore diffusivity κ_x outside the surf zone is equal to half of the slope of the best-fit line. (For interpretation of the references to color in this figure legend, the reader is referred to the Web version of this article.)

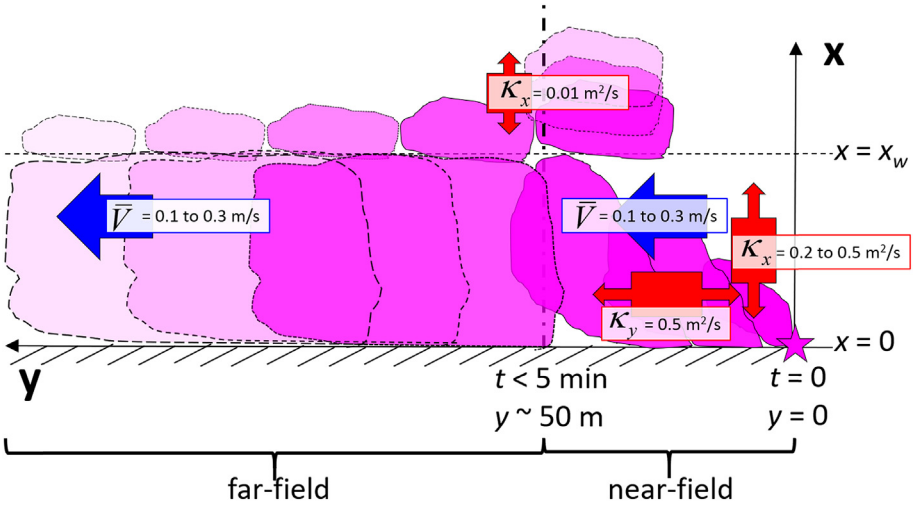

Fig. 12. A conceptual diagram of the mixing and transport of dye (pink) that was observed on the sandy, steep beach at CRSB. Dye released as an instantaneous point source at the shoreline (star at $t = 0$, $x = 0$, $y = 0$), which is assumed to be rapidly vertically well-mixed, initially dispersed in two dimensions in the near-field ($t < 5$ min, $y < 50$ m), where advection and diffusion processes were important; then when the dye was completely mixed across the surf zone, the dye was transported due to advection in the far-field ($t > 5$ min, $y > 50$ m). In the near-field, the dye spread in the cross-shore (κ_x) by turbulent diffusion due to breaking waves and spread in the alongshore (κ_y), while also being advected downstream with the surfzone averaged alongshore current ($\bar{V}$). In the far-field, the dye was advected downstream with the surfzone averaged alongshore current ($\bar{V}$). Dye leaked cross-shore to outside the surfzone ($x > x_w$) in manner not completely understood. The dye outside the surfzone moved as a constant patch, with a small amount of cross-shore spreading. (For interpretation of the references to color in this figure legend, the reader is referred to the Web version of this article.)

advected seaward. On a steep beach the surfzone can be viewed as a swash zone where plunging or surging breakers run-up the beach face at the incident wave angle, and then run-down the beach face owing to gravity. This zig-zag of the swash constitutes the alongshore current. Often the run-down collides with an incoming wave that results in a collapsing breaker at the step in the profile creating a large amount of turbulence and mixing. It appears that on the subsequent surging breaker the dye that was violently mixed by the collapsing breaking wave was left behind offshore resulting in dye seeping offshore and escaping the surfzone (see Fig. 3). Once the dye is offshore, it disperses slowly owing to the low ambient turbulence.

5.1.2. Far-field mixing and transport

In the far-field region, the dye in the surfzone was completely mixed (Fig. 12). Observations of $M(y)$ decayed in the alongshore more gradually than in the near-field, as the dye was observed to be predominantly advected alongshore with $\bar{V}$ (Fig. 8). Additionally, the dye continued to be dispersed alongshore and cross-shore in the far-field, both inside and outside the surfzone. These findings are consistent with advectively dominated transport in the far field on dissipative beaches (Grant et al., 2005), but the alongshore distance to the far field is much shorter at CRSB.

5.2. Effect of local bathymetry on alongshore surfzone transport and cross-shore exchange

The observed decrease in $\bar{V}$ with distance alongshore to the south (Fig. 8a) could be explained by the decrease in wave angle relative to the shoreline with distance alongshore to the south due to the curvature of the bay. Waves coming from the north and driving the alongshore

current to the south tend to be more shore-normal at the southern end of the experiment area and therefore force weaker alongshore currents. This would result in a relative convergence of alongshore flows in the surfzone and require an offshore directed flow. In numerical model simulations investigating biological transport during the CRSB experiment under the same conditions discussed here, Fujimura et al., (2013) found that the alongshore current is to the south and follows the contours of the embayed beach until approximately $y = 100$ m, where the current moves predominantly offshore apparently as a rip current. The southern end of the alongshore array of dye sensors is located where this change in current from alongshore to offshore occurs, which could explain the decrease in $V(y)$ with distance alongshore.

6. Summary

Nearshore processes of waves and currents and their impact on mass transport and cross-shore exchange were observed for a sandy, steep, reflective beach at Carmel River State Beach, California. Owing to the steep slope (1/8) of the beach, plunging-collapsing waves broke close to the shoreline resulting in an intense shore break and a large swash zone rather than a typical surfzone generally associated with dissipative beaches. Dye was released as a slug in the surfzone as a tracer and an alongshore array of stationary dye sensors and repeated cross-shore transects performed by swimmers equipped with dye sensors at multiple alongshore locations were used to measure the temporal and spatial dye concentration evolution.

Visual dye observations indicate that the dye quickly mixed vertically and dispersed in the cross-shore, completely saturating the narrow surfzone within minutes. Dye concentration time series measured by an alongshore array of stationary dye sensors inside the surfzone revealed sharp-rising, narrow spikes of dye concentration that decayed rapidly near the dye release location, which broadened and decayed more slowly and decreased in peak concentration with alongshore distance downstream from the dye release location. Mixing and transport processes occur in two stages on the steep beach, which are summarized in a conceptual diagram in Fig. 12. Inside the surfzone in the near-field, within approximately 50 m alongshore from the dye release location, dye was mixed in the cross-shore by turbulent diffusion due to breaking waves (κ_x = 0.2–0.5 m^2 s-1) and was advected downstream with the mean alongshore surfzone current ($\bar{V}$ = 0.1–0.3 m s-1) and spread in the alongshore (κ_y = 0.5 m^2 s-1). Inside the surfzone in the far-field, once the dye was completely mixed vertically and in the cross-shore, the dye continued to be transported alongshore with the mean alongshore current and spread in the alongshore, while also being slowly transported offshore. The mechanism(s) responsible for transport of dye from inside the surfzone to offshore is not understood. Outside the surfzone, the cross-shore diffusion coefficient κ_x was 0.01 m^2 s-1 indicating the dye was spreading more slowly than inside the surfzone, and that it was essentially moving offshore as a constant patch.

The mixing and transport processes observed on this steep beach resemble those observed on dissipative beaches, with some distinct differences. Similar to the exponential decay of tracer measured on several advection-dominated dissipative beaches (Inman et al., 1971; Boehm, 2003; Grant et al., 2005), measured dye mass decreased by a value of 1/e within the near field on the steep beach. In the far-field, the mass transport was dominated by advection, similar to that on dissipative beaches under alongshore current conditions; however, the far-field on the steep beach was reached in a much shorter alongshore distance than on dissipative beaches. The measured diffusion coefficients on this steep beach are smaller than values previously measured on dissipative beaches, both inside and outside the surfzone. These results indicate the differences in how material is transported and mixed on steep beaches compared to dissipative beaches, which has implications on material dispersion and residence times in the surfzone.

Acknowledgements

This work was supported by the National Science Foundation (OCE-0926750), and the instrumentation used during the field work was funded by the Office of Naval Research (ONR DURIP #N0001409WR20268). J. Brown was supported by the Department of Defense through the National Defense Science and Engineering Graduate (NDSEG) Fellowship. We would like to thank the California State Parks department and the community of Carmel by the Sea for their cooperation during the field experiment, and we would like to thank the many people who assisted in collecting the field data: Keith Wyckoff, Ron Cowen, Bill Swick, Casey Gon, Dave Watson, Atsushi Fujimura, Benjamin Straubhaar, Marley Jarvis, Chris Griesemer. We would also like to thank our reviewers and Falk Feddersen for their comments and contributions in improving this manuscript.

References

Battjes, J.A., 1975. Modeling of Turbulence in the Surf Zone, Paper Presented at Symposium on Modeling Technology. Am. Soc. of Civ. Eng., San Francisco, CA.
Boehm, A.B., 2003. Model of microbial transport and inactivation in the surf zone and application to field measurements of total coliform in northern orange county, California. Environ. Sci. Technol. 37 (24), 5511–5517.
Brown, J.W., MacMahan, J.H., Reniers, A.J.H.M., Thornton, E.B., 2009. Surf zone diffusivity on a rip-channeled beach. J. Geophys. Res. 114 (C11015). https://doi.org/10.1029/2008JC005158.
Brown, J.A., MacMahan, J.H., Reniers, A.J.H.M., Thornton, E.B., 2015. Field observations of surf zone-inner shelf exchange on a rip-channeled beach. J. Phys. Oceanogr. 45, 2339–2355.
Castelle, B., Coco, G., 2013. Surf zone flushing on embayed beaches. Geophys. Res. Lett. 40 (10), 2206–2210.
Castelle, B., Reniers, A.J.H.M., MacMahan, J.H., 2014. Bathymetric control of surf zone retention on a rip-channeled beach, *Oc*. Dynamics 64 (8), 1221–1231.
Clark, D.B., Feddersen, F., Omand, M.M., Guza, R.T., 2009. Measuring fluorescent dye in the bubbly and sediment-laden surfzone. Water Air Soil Pollut. 204 (1–4), 103–115.
Clark, D.B., Feddersen, F., Guza, R.T., 2010. Cross-shore surfzone tracer dispersion in an alongshore current. J. Geophys. Res. 115 (C10035). https://doi.org/10.1029/2009JC005683.
Feddersen, F., 2012. Scaling surf zone turbulence. Geophys. Res. Lett. 39 (L18613). https://doi.org/10.1029/2012GL052970.
Fong, D.A., Stacey, M.T., 2003. Horizontal dispersion of a near-bed coastal plume. J. Fluid Mech. 489, 239–267.
Fischer, H.B., List, E.J., Koh, R.C.Y., Imberger, J., Brooks, N.H., 1979. Mixing in Inland and Coastal Waters. Academic Press, New York.
Fujimura, A., Reniers, A.J.H.M., Paris, C.B., Shanks, A.L., MacMahan, J.H., Morgan, S.G., 2013. Slope-dependent biophysical modeling of surf zone larva transport. In: Proceedings Coastal Dynamics, vol. 13. pp. 73.
Fujimura, A., Reniers, A.J.H.M., Paris, C.B., Shanks, A.L., MacMahan, J.H., Morgan, S.G., 2014. Numerical simulations of larval transport into a rip-channeled surf zone. Limnol. Oceanogr. 59, 1434–1447.
Garcez Faria, A.F., Thornton, E.B., Lippmann, T.C., Stanton, T.P., 2000. Undertow over a barred beach. J. Geophys. Res. 105 (C7), 16999–17010.
Given, S., Pendleton, L.H., Boehm, A.B., 2006. Regional public health cost estimates of contaminated coastal waters: a case study of gastroenteritis at Southern California beaches. Environ. Sci. Technol. 40 (16), 4851–4858.
Grant, S.B., Kim, J.H., Jones, B.H., Jenkins, S.A., Wasyl, J., Cudaback, C., 2005. Surf zone entrainment, along-shore transport, and human health implications of pollution from tidal outlets. J. Geophys. Res. 110 (C10025). https://doi.org/10.1029/2004JC002401.
Hally-Rosendahl, K., Feddersen, F., Guza, R.T., 2014. Cross-shore tracer exchange between the surfzone and inner-shelf. J. Geophys. Res. 119, 4367–4388. https://doi.org/10.1002/2103JC009722.
Hally-Rosendahl, K., Feddersen, F., Clark, D.B., Guza, R.T., 2015. Surfzone to inner-shelf exchange estimated from dye tracer balances. J. Geophys. Res. 120, 6289–6308. https://doi.org/10.1002/2105JC010844.
Hally-Rosendahl, K., Feddersen, F., 2016. Modeling surfzone to inner-shelf tracer exchange. J. Geophys. Res. Ocean. 121, 4007–4025. https://doi.org/10.1002/2015JC011530.
Harris, T.F.W., Jordaan, J.M., McMurray, W.R., Verwey, C.J., Anderson, F.P., 1963. Mixing in the surf zone. Int. J. Air Water Pollut. 7, 649–667.
Inman, D.L., Tait, R.J., Nordstrom, C.E., 1971. Mixing in the surfzone. J. Geophys. Res. 76 (15), 3493–3514.
Kumar, N., Feddersen, F., 2017a. The effect of Stokes drift and transient rip currents on the inner shelf. Part I: No stratification. J. Phys. Oceanogr. 47, 227–241.
Kumar, N., Feddersen, F., 2017b. The effect of Stokes drift and transient rip currents on the inner shelf. Part II: with stratification. J. Phys. Oceanogr. 47, 243–260.
Kumar, N., Feddersen, F., 2017c. A new offshore transport mechanism for shoreline-released tracer induced by transient rip currents and stratification. Geophys. Res. Lett. 44, 2843–2851. https://doi.org/10.1002/2017GL072611.
Lentz, S.J., Fewings, M., Howd, P., Fredericks, J., Hathaway, K., 2008. Observations and a

model of undertow over the inner continental shelf. J. Phys. Oceanogr. 38, 2341–2357.
MacMahan, J.H., Brown, J.W., Brown, J.A., Thornton, E.B., Reniers, A.J.H.M., Stanton, T.P., Henriquez, M., Gallagher, E., Morrison, J., Austin, M.J., Scott, T.M., Senechal, N., 2010. Mean Lagrangian flow behavior on an open coast rip-channeled beach: a new perspective. Mar. Geol. 268, 1–15.
Morgan, S.G., Shanks, A.L., MacMahan, J.H., Reniers, J.H.M., Feddersen, F., 2018. Planktonic subsidies to surf-zone and intertidal communities. Annu. Rev. Mar. Sci. 10, 345–369.
Raubenheimer, B., Guza, R.T., 1996. Wave transformation across the inner surf zone. J. Geophys. Res. 101 (C10) 25,589-25,597.
Reniers, A.J.H.M., Thornton, E.B., Stanton, T.P., Roelvink, J.A., 2004. Vertical flow structure during Sandy Duck: observations and modeling. Coast. Eng. 51, 237–260.
Reniers, A.J.H.M., MacMahan, J.H., Thornton, E.B., Stanton, T.P., Henriquez, M., Brown, J.W., Brown, J.A., Gallagher, E., 2009. Surf zone surface retention on a rip-channeled beach. J. Geophys. Res. 114, C10010. https://doi.org/10.1029/2008JC005153.
Reniers, A.J.H.M., MacMahan, J.H., Beron-Vera, F.J., Olascoaga, M.J., 2010. Rip-current pulses tied to Lagrangian coherent structures. Geophys. Res. Lett. 37, L05605. https://doi.org/10.1029/2009GL041443.
Sheremet, A., Guza, R.T., Elgar, S., Herbers, T.H.C., 2002. Observations of nearshore infragravity waves: seaward and shoreward propagating components. J. Geophys. Res. 107 (C8). https://doi.org/10.1029/2001JC000970.
Smart, P.L., Laidlaw, I.M.S., 1977. Evaluation of some fluorescent dyes for water tracing. Water Resour. Res. 13 (1), 15–33.
Spydell, M.S., Feddersen, F., Guza, R.T., Schmidt, W.E., 2007. Observing surf-zone dispersion with drifters. J. Geophys. Oceanogr. 37 (12), 2920–2939.
Spydell, M.S., Feddersen, F., 2012. A Lagrangian stochastic model of surf zone drifter dispersion. J. Geophys. Res. 117 (C03041). https://doi.org/10.1029/2011JC007701.
Suanda, S., Feddersen, F., 2015. A self-similar scaling for cross-shore exchange driven by transient rip currents. Geophys. Res. Lett. 42, 5427–5434.
Wright, L.D., 1982. Field observations of long-period surf zone oscillations in relation to contrasting beach morphologies. Aust. J. Mar. Freshw. Res. 33, 181–201.